Available online at www.sciencedirect.com

ScienceDirect

IFAC Papers Online CONFERENCE PAPER ARCHIVE

IFAC PapersOnLine 56-2 (2023) 1970–1976

Power Sharing Control of High Speed Railway Traction Networks Supplied by Dual End Substations

Peiliang Sun * **Kang Li** * **Chen Xing** * **Shihao Zhao** *

* *School of Electronic and Electrical Engineering, University of Leeds, Leeds, LS2 9JT, UK (e-mail: k.li1@leeds.ac.uk)*

Abstract: This paper presents a novel power sharing control for high speed railway traction networks which are supplied continuously by dual end substations without the neutral section. The power sharing between two substations is realised by droop control where the droop coefficients are updated based on the actual traction load distribution for a given specific active power sharing ratio, while the power sharing ratio is optimised for the least conductor line losses under the light-medium load condition. For the heavy load condition, power at both substations are more balanced so that the substation capacity can be set at a lower rating. The proposed approach is tested on a simplified single-track network model which supports continuous traction dynamics and auto-transformer connection, and simulation results confirm that the proposed method has advantages of increasing the supply distance compared with the conventional transformer substation scheme. It offers greater power supply capacity than the fixed frequency substation control scheme, and it also achieves less power losses than the equal power sharing strategy proposed in the existing studies.

Keywords: Railway power supply, continuous power supply, static frequency converter, traction network.

1. INTRODUCTION

Transportation is among the most challenging sectors for decarbonization, and as the energy sector is embracing significant renewable penetration, the electrified railway is becoming an environmentally more friendly means of transportation than on-road vehicles and air transport (Sun et al., 2020). The ac power supply scheme is the most consolidated technology where the high voltage power source provided by the utility grid is reduced to a suitable level and is then fed to the railway conductors. The main electrical schemes in AC electric railway are 15 kV $16\frac{2}{3}$ Hz and 25 kV 50 Hz which are widely used in most countries. AC feeder transformers are essential in the conventional substations. Generally the transformer connects between three phase AC grid and single phase overhead line system (Bagnall et al., 2014). The current trend is that the traction power supply system (TPSS) is gradually evolving towards a smarter railway grid using converter-based system (Serrano-Jiménez et al., 2017). Fig. 1 illustrates the single-end substation TPSS and dual-end static frequency converter (SFC) based TPSS.

It is easier to use parallel feeding in DC railway network where distributed energy sources can be directly connected to the DC line (Gómez-Expósito et al., 2013), even the unidirectional diode rectifier substations can be connected in parallel to share traction loads (Hao et al., 2020). The idea of continuous feeding scheme for AC railway network can be found in some literature (Perin et al., 2018; Buttery et al., 2016; Krastev et al., 2016; Chen et al., 2015). Because the power angle of transformer station output is uncontrollable, power electronic converters are necessary to control the parallel feeding in the AC traction network.

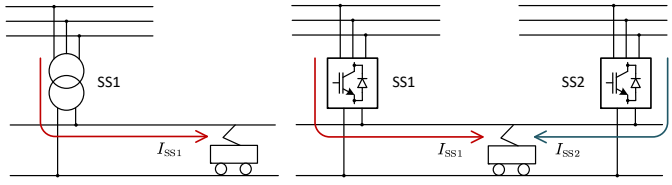

(a) Single end power supply (b) Dual end power supply

Fig. 1. Traction network power supply

There are two types of parallel feeding schemes: 1) synchronised control without actively changing the power angle between stations; 2) equal sharing by communicated centralised controller or by droop control method. Static frequency converter (SFC) has been developed to replace conventional transformer stations in the railway power supply system. Although the SFC is compatible with power sharing scheme, in the current supply schemes, the single phase output voltages are controlled to the same phase angle, i.e. these SFCs are strictly synchronised (Sharifi, 2018). To achieve power sharing control in the AC traction network, the droop control method is widely used (Chen et al., 2015). Droop control in AC supply has two degrees of freedom: the voltage magnitude and phase angle (Krastev et al., 2016).

⋆ This work is partially funded by the Ofgem SIF on 'Railway Multi-energy Hub Networks For Integrated Green Mobility in Renewable Energy'.

10.1016/j.ifacol.2023.10.1090

In (Krastev et al., 2016), a train is placed at 17.5 km to the substation in a three feeder station network. These three feeder stations are controlled by one droop control profile and shares active power almost equally. (Sharifi et al., 2016) explained that for a train between two SFC continuous feeding condition, the train draws "a percentage of power substantially inversely proportional to the distance from each substation". Sharifi et al. proposed a control system that enables each train to draw 50% of the traction power from each station in all positions along the network. This equal share principle will help to reduce the rating of each SFC station in future system or improving the capacity in the SFC installed system. In (Sharifi, 2018), a 'mesh feeding' scheme is proposed and a central smart controller is used to provide equal shared active power and limit the reactive power. Researchers also investigated the droop control for equal load sharing between two cascaded 3-level converters in parallel (Han et al., 2017). However, in the previous research, the traction networks are simplified into single node resistor and inductor between trains and stations (Han et al., 2017; Sharifi et al., 2016). The traction loads are often analysed in a fixed position rather than modeling the train continuously moving on the rail track (Perin et al., 2018; Krastev et al., 2016).

This paper envisages a future application scenario of using multiple substations to support railway traction network, viz. using parallel connected SFCs for continuous power supply without the need of a neutral section between two substations. The main contribution are as follows:

- To better represent the railway network and the dynamic nature of the traction load, a simulation platform to model the SFC parallel feeding is built. A special adaptive droop controller is designed to achieve an active power sharing between two SFC substations for less power loss and greater supply capacity.
- A special adaptive droop controller is designed to achieve an active power sharing between two SFC substations for less power loss and greater supply capacity.

The remainder of this paper is arranged as follows. Section 2 presents the modelling considerations of the traction network system; Section 3 detailes the power sharing strategy design, and the droop controller design is given in Section 4. Section 5 discusses the simulation results and Section 6 concludes the paper.

2. MODELLING OF THE TRACK RAILWAY POWER SUPPLY NETWORK

The modelling of the AC traction work system is explained in this section. Each of the constituent parts are modelled by equivalent circuits in MATLAB/Simulink time domain simulation environment. Modelling assumptions are listed as follows:

- Nonlinear properties such as magnetic saturation, thermal effect in transformers and reactors are ignored.
- Harmonic components are not considered in modelling power converters and all AC component are controlled to produce fundamental frequency waves.
- The high speed train is assumed to have unity power factor in steady state. Ideally no reactive power are to be produced by traction load [1] .

2.1 Substation and transformer model

(1) *Static frequency converter:* SFC power supply station can be realised in different topology with different types of power electronics components (Steimel, 2012; Shimizu et al., 2014; Taffese et al., 2020). Although different in topologies, SFCs are controlled as voltage sources. So, the power converter dynamics are simplified as a controlled voltage source where the supply terminal voltage is controlled by reference signals.
(2) *Output transformer:* Output transformers or output reactors may or may not be needed depending on the specific SFC design. In this work, a linear three winding transformer is used to connect the SFC with the AT double voltage system.
(3) *Autotransformer:* The autotransformer stations are described by two winding transformers with 1:1 turn ratio, and a two-winding linear transformer model is used to represent an AT station.

2.2 Conductor line model

The network comprises multiple conductor lines such as contact wire, messenger wire, feeder wire, protection wire, etc. A set of model parameters taken from a heavy-duty electrified railway line is selected as the network model (Junwen et al., 2010). This complex network can be simplified as a parallel multi-conductor system and represented by a mutual impedance model. The parameters of mutual impedance model need to be updated at each sampling time according to different distance between two adjacent trains. Therefore, a variable multi-conductor line model is required.

Impedance values are derived using Carson theory. A detailed model of double track system has up to 8 to 10 conductors. To simplify the problem and to preserve the AT connection feature, a single-track line three conductor model is used in this study. The circuit model is described in (1)

$$\boldsymbol{u}_{\mathrm{N}} = \frac{\mathrm{d}}{\mathrm{d}t}\boldsymbol{\psi}_{\mathrm{N}} + \boldsymbol{R}_{\mathrm{N}}\boldsymbol{i}_{\mathrm{N}} \approx \boldsymbol{L}_{\mathrm{N}}\frac{\mathrm{d}}{\mathrm{d}t}\boldsymbol{i}_{\mathrm{N}} + \boldsymbol{R}_{\mathrm{N}}\boldsymbol{i}_{\mathrm{N}}, \tag{1}$$

where $\boldsymbol{u}_{\mathrm{N}} = [u_{\mathrm{T}}\ u_{\mathrm{F}}\ u_{\mathrm{R}}]^{\mathrm{T}}$ and $\boldsymbol{i}_{\mathrm{N}} = [i_{\mathrm{T}}\ i_{\mathrm{F}}\ i_{\mathrm{R}}]^{\mathrm{T}}$ represent the voltage and current in each node and the subscript '$_{\mathrm{T}}$' represents traction contact line, '$_{\mathrm{F}}$' is for feeder line, and '$_{\mathrm{R}}$' is for rail. The inductance and resistance matrices having self and mutual impedance respect to different distance value (D) are defined in (2)

$$\begin{aligned} \boldsymbol{L}_{\mathrm{N}} &= D\begin{bmatrix} L_{\mathrm{T}} & L_{\mathrm{TF}} & L_{\mathrm{TR}} \\ L_{\mathrm{TF}} & L_{\mathrm{F}} & L_{\mathrm{FR}} \\ L_{\mathrm{TR}} & L_{\mathrm{FR}} & L_{\mathrm{F}} \end{bmatrix} \\ \boldsymbol{R}_{\mathrm{N}} &= D\begin{bmatrix} R_{\mathrm{T}} & R_{\mathrm{TF}} & R_{\mathrm{TR}} \\ R_{\mathrm{TF}} & R_{\mathrm{F}} & R_{\mathrm{FR}} \\ R_{\mathrm{TR}} & R_{\mathrm{FR}} & R_{\mathrm{F}} \end{bmatrix} \end{aligned} \tag{2}$$

The multi-conductor is modelled by a set of controlled current sources as expressed in (4). According to the di-

[1] Due to the phase locked loop delay and sampling errors, tiny amount of reactive power exists.

Table 1. Substation output transformer parameter

Nominal power rating	35 MW	Terminal voltage	27.5 kV
Short-circuit ratio	8%	Impedance ratio	1:4

mensional analysis, current state matrix is constant which does not change with the conductor length, however the multi-conductor input matrix $\boldsymbol{A}_{\mathrm{N}}$ is inversely proportional to the distance and has the dimension of 1/(m·H).

$$\frac{\mathrm{d}}{\mathrm{d}t}\boldsymbol{i}_{\mathrm{N}} = \boldsymbol{A}_{\mathrm{MC}}\boldsymbol{i}_{\mathrm{N}} + \boldsymbol{B}_{\mathrm{MC}}\boldsymbol{u}_{\mathrm{N}}, \tag{3}$$

$$\begin{aligned}\boldsymbol{A}_{\mathrm{MC}} &= -\begin{bmatrix} L_{\mathrm{T}} & L_{\mathrm{TF}} & L_{\mathrm{TR}} \\ L_{\mathrm{TF}} & L_{\mathrm{F}} & L_{\mathrm{FR}} \\ L_{\mathrm{TR}} & L_{\mathrm{FR}} & L_{\mathrm{F}} \end{bmatrix}^{-1} \begin{bmatrix} R_{\mathrm{T}} & R_{\mathrm{TF}} & R_{\mathrm{TR}} \\ R_{\mathrm{TF}} & R_{\mathrm{F}} & R_{\mathrm{FR}} \\ R_{\mathrm{TR}} & R_{\mathrm{FR}} & R_{\mathrm{F}} \end{bmatrix}, \\ \boldsymbol{B}_{\mathrm{MC}} &= \frac{1}{D}\begin{bmatrix} L_{\mathrm{T}} & L_{\mathrm{TF}} & L_{\mathrm{TR}} \\ L_{\mathrm{TF}} & L_{\mathrm{F}} & L_{\mathrm{FR}} \\ L_{\mathrm{TR}} & L_{\mathrm{FR}} & L_{\mathrm{F}} \end{bmatrix}^{-1}\end{aligned} \tag{4}$$

2.3 Traction load model

The CRH380BL is selected as the high-speed train model to generate power load according to the traction profile. One CRH380BL train has 16 carriages. The maximum operation speed is 310 km/hr with nominal total mass 972.8 t and maximum power for traction 18.4 MW

According to (Hu et al., 2015; Shan et al., 2017), traction force (F_{tr}) curve at full power is described by (5) which has constant power region and constant torque region. Braking force (F_{br}) curve at full power is expressed in (6). The resistive force (F_{re}) curve is approximated by "Davis" equation and the straight horizontal track scenario is formulated in (7).

$$F_{\mathrm{tr}} = \begin{cases} 454 & [\mathrm{kN}]\ v \le 40.56\,\mathrm{m/s} \\ 18400/v & [\mathrm{kN}]\ v > 40.56\,\mathrm{m/s} \end{cases} \tag{5}$$

$$F_{\mathrm{br}} = \begin{cases} 326.6v & [\mathrm{kN}] \quad v \le 1.39\,\mathrm{m/s} \\ 454 & [\mathrm{kN}]\ 1.39\,\mathrm{m/s} < v \le 40.56\,\mathrm{m/s} \\ 18400/v & [\mathrm{kN}] \quad v > 40.56\,\mathrm{m/s} \end{cases} \tag{6}$$

$$F_{\mathrm{re}} = 0.000755Mg + 192.55v' + 11.6\left(v'\right)^2\ [\mathrm{N}], \tag{7}$$

where M is the train mass (set to 900 t), g is the gravitational acceleration, and v' is the sum of train speed and wind speed $v' = v + v_{\mathrm{wind}}$.

2.4 Simulation system design

The main model parameters of the traction network are listed in Tables 1, 2 and 3.

To simulate the dynamic traction load, a model of 2 trains and 1 AT station is built as shown in Fig. 2 for simplicity. Both trains depart from left substation to the right. Each AT station is in shunt connection to the network which splits the network into two sections. In the simulation the train model cannot 'pass' through these shunt connections. To solve this issue, two trains are assigned in each section and one multi-conductor model is connected between each model.

3. POWER SHARING STRATEGY DESIGN

Three key aspects are mainly considered in the power sharing control design: Joule effect losses on the conductor lines, voltage drop measured at traction load side and substation rating limit.

Table 2. Autotransformer parameter

Nominal power rating	16 MW	Terminal voltage	27.5 kV
Short-circuit ratio	1.6%	Impedance ratio	1:4

Table 3. Multiconductor model parameter

Reactance data (50Hz)			
X_{T}	0.6019 Ω/km	X_{TF}	0.3272 Ω/km
X_{F}	0.7020 Ω/km	X_{TR}	0.3276 Ω/km
X_{R}	0.4617 Ω/km	X_{FR}	0.3402 Ω/km
Resistance data			
R_{T}	0.1445 Ω/km	R_{TF}	0.0515 Ω/km
R_{F}	0.2234 Ω/km	R_{TR}	0.0481 Ω/km
R_{R}	0.1098 Ω/km	R_{FR}	0.0414 Ω/km

3.1 Power sharing strategy for single train

Conventionally, two substations are supplying in parallel with the synchronised phase angle. In this power supply scheme, the substation having loads nearby provides most of the power and the substation that is distant from the train provides less power. In the AT connected multi-conductor model, it is difficult to derive close-form expression of optimal power sharing strategy for the least power losses. Numerical calculation is used to assess the performance of different power sharing ratios. Considering the nonlinearity, the following optimisation procedure (8) is solved using sequential quadratic programming (SQP) to search for the optimal active power ratio between two substations. Only 0 to 30 km are calculated because the system is modelled to be symmetric.

$$\begin{aligned} \underset{P_1,P_2}{\text{minimise}} \quad & (P_1 + P_2 - P_{\mathrm{Tr}}) \\ \text{s.t.} \quad & V_{\mathrm{Tr}} \ge 22\,\mathrm{kV}. \\ & P_{\mathrm{Tr}} = 10, 20, \ldots 50\,\mathrm{MW}. \\ & D_1 = 0, 1, 2, \ldots 30\,\mathrm{km}. \end{aligned} \tag{8}$$

where P_1 and P_2 are the power of the two substations respectively, P_{Tr} is the actual required traction power.

The result is shown in Fig. 3. The substation which is nearer to the load supplies more power. And two SFCs share an equal amount of the power when the train is in the midpoint. However, the ratio is not strictly inverse to the distance. In the heavy load condition, the ratio of power supply differences decreases because the network voltage has to be maintained above 22kV as set in the constraints.

In reality, a single high-speed train will not likely exceed 20 MW. The averaged ratio curve of 10, 20, 30 MW load is used and fitted by an exponential function (9), where D_1 is the train distance to the left SS1 substation and k is the power ratio of P_1/P_2.

$$\begin{aligned} k\left(D_1\right) &= a \times e^{bD_1} + c \times e^{dD_1}, \\ & a = 1.554, b = -0.1955, c = 4.026, d = -0.04656 \end{aligned} \tag{9}$$

3.2 Power sharing strategy for three trains

To design the power sharing strategy for multiple-trains condition, three-train scenarios are considered in the test.

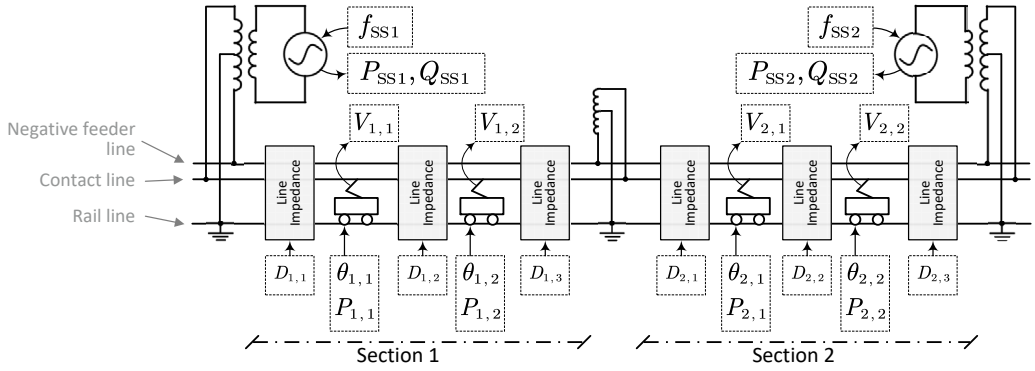

Fig. 2. Illustration of a simplified two section traction network simulation model with dual-end parallel feeding

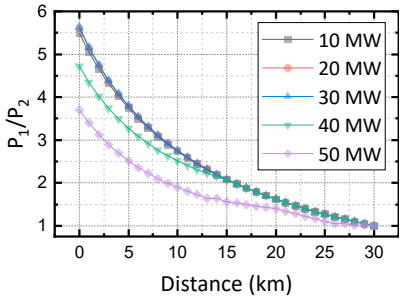

Fig. 3. Optimal power ratio for single traction load

1000 random combinations of different locations and power loads are generated. In each instance, the optimal power sharing ratio P1/P2 is searched using the same approach (10) in the previous "single train case".

$$\begin{aligned} \underset{P_1,P_2}{\text{minimise}} \quad & (P_1 + P_2 - \sum_{i=1}^{3} P_{\mathrm{Tr},i}) \\ \text{subject to} \quad & V_{x,y} \geq 22\,kV, && x = 1,2.\ y = 1,2,3. \\ & 0 \leq P_{x,y} \leq 15\,\mathrm{MW}, && x = 1,2.\ y = 1,2,3. \\ & 0 \leq D_y \leq 30\,\mathrm{km}, && y = 1,2,3. \\ & D_1 < D_2 < D_3\,. \end{aligned} \tag{10}$$

The optimisation results provide a series of optimal power ratios for different multiple load conditions. If the non-linear effect of power transmission can be ignored, we can reuse the answer found in the single train case. Using (11), an equivalent distance can be calculated. A virtual single train distance can be derived to represent the multiple trains' condition. Based on this approximation, the optimal power sharing ratio can be calculated by (12) where the function $k(D')$ is given in (9).

$$D' \approx \begin{cases} \frac{\Sigma_i P_i D_i}{\Sigma_i P_i} & \Sigma_i P_i \neq 0\,; \\ 30 & \Sigma_i P_i = 0\,. \end{cases} \tag{11}$$

$$\left(\frac{P_1}{P_2}\right)_{\mathrm{opt}} = \begin{cases} k\,(0) & D' < 0\,; \\ k\,(D') & 0 \leq D' \leq 60\,; \\ k\,(60) & D' > 60\,. \end{cases} \tag{12}$$

The power ratio generated by this approximated approach which transforms three-train case into single-train case has less than 1% difference with the original optimisation result. In this approach, the three-train scenario is converted to the single-train case.

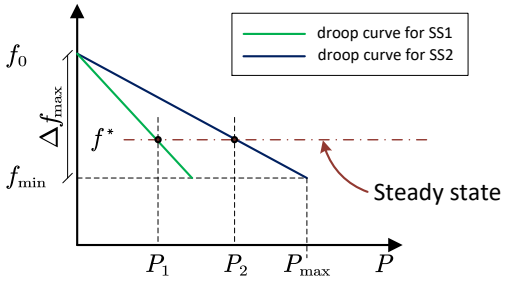

Fig. 4. Frequency droop line for two substations

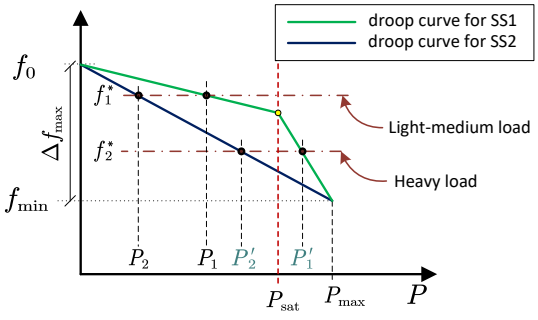

Fig. 5. Modified droop curve with power saturation protection

4. DROOP CONTROLLER PARAMETER DESIGN

The proposed power sharing is realised through frequency droop control. As shown in Fig. 4, each substation has a frequency droop line with different slope values. In the steady state, the voltage frequency is converged to f^* first then using the corresponding droop line pattern. As shown in Fig. 4, SS1 supplies traction power with P_1 active power and SS2 is providing P_2.

The simple droop curve in Fig. 4 shows that the frequency reference follows $f^* = f_0 - k_{\mathrm{d}}P$, $f_0 = 50\,\mathrm{Hz}$ where P_1, P_2 are the measured active power and $k_{\mathrm{d1}}, k_{\mathrm{d2}}$ is the droop coefficient. In the steady state, two substations have the same output voltage frequency, namely $f_1^* = f_2^*$, so the active power ratio is strictly inverse proportional to the droop coefficient ratio. The active power sharing ratio defined in (12) can be achieved by changing the droop coefficient value.

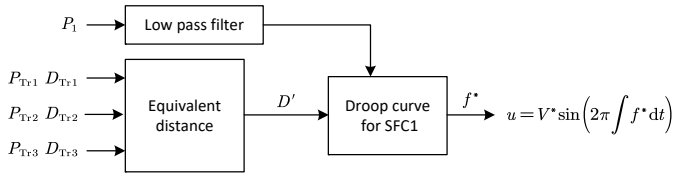

Fig. 6. Droop control scheme for SS1 substation

$$k_{d1} P_1 = k_{d2} P_2 \quad \Rightarrow \quad \frac{k_{d1}}{k_{d2}} = \frac{P_2}{P_1} \tag{13}$$

However, with a simple linear droop characteristic, overloading situations may arise in high power demand situations. A modified droop curve to limit the maximum output power is designed and illustrated in Fig. 5.

The proposed droop control scheme is summarized in Fig. 6. Firstly, the equivalent load distance is calculated then based on the active power and distance information, the frequency reference is interpolated from the designed droop curve. Then each substation is controlled to track the voltage reference.

A parameter sweep analysis is used to evaluate the eigenvalue: 1) LPF time constant T_f changes from 1/25 s to 1/200 s, 2) Droop curve saturation set point P_{sat}/P_{max} is set from 0.5 to 0.9, 3) Traction load power is set from 10 MW to 50 MW, 4) Load distance to left substation is varying from 0 to 30 km. In each combination instance, eigenvalues of the system matrix have been calculated. None of the results has positive real parts which shows the droop method controlled power supply system is stable.

5. SIMULATION RESULT DISCUSSION

Four types of power supply strategies are selected in the simulation for comparison purpose.

(1) Single substation supply:
Similar to the conventional power supply scheme, only one substation supplies the whole arm.
(2) Two substations fixed frequency:
Two substations are strictly synchronised with fixed 50 Hz voltage supply reference without any load sharing control.
(3) Two substation equal sharing:
Two substations use the same droop coefficient of 0.5 Hz/p.u.. So two substations share exactly the same amount of active power no matter the load condition.
(4) The proposed adaptive droop curve:
The proposed droop control power supply scheme given in this paper. The droop coefficient for each substation varies according to the load condition.

5.1 Comparison of power supply schemes - single traction load

Firstly, a 10 MW constant load is continuously moving from SS1 to SS2 in 1080 s (200 km/hr). Fig. 7 compares the active power result, where Fig. 7a shows that all the three dual-end supply schemes have lower power losses than the single substation supply scheme because the current loading is reduced. Equal sharing supply exhibits the same

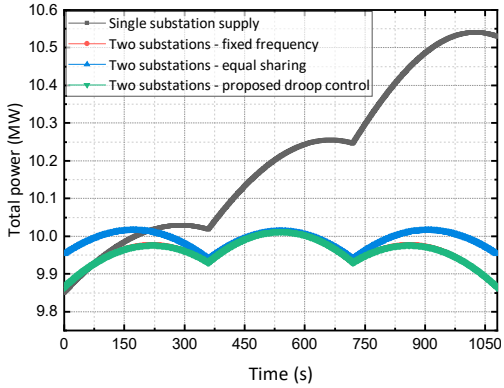

(a) Sum of active power ($P_{SS1} + P_{SS2}$)

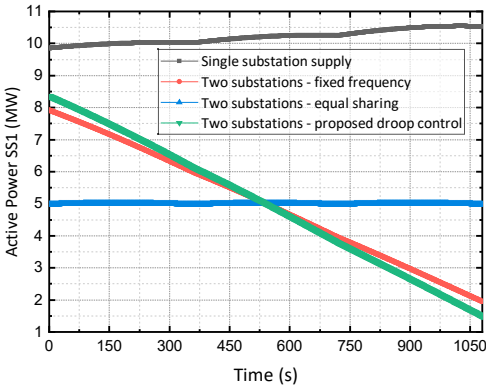

(b) Active power of SS1 (P_{SS1})

Fig. 7. Comparison of active power consumption (single traction load)

power loss as other dual end supply methods when the traction load is located in the middle of two SFCs. But when the train is near to one substation, equal sharing scheme leads to greater losses because of its strict equal share principle.

In the light load (10 MW) scenario, the proposed droop control supply has almost the same energy loss as the fixed frequency approach. And both of these two methods have the least energy loss on the conductor lines. Fig. 7b shows the active power consumption on SS1 substation. In the equal sharing method, active power provided by SS1 is maintained about 5 MW. Here, both the proposed method and fixed frequency method have similar load requirement.

Fig. 8 shows the voltage frequency. Because the load is constant, the frequency keeps nearly constant in equal sharing method. The proposed droop control method has variable frequency between equal sharing and other methods. Note that when the traction is in the middle location, the proposed method is identical to the equal sharing approach.

5.2 Comparison of power supply schemes - three-train scenario

To test the limit of the proposed droop control supply scheme in a more complex load condition, the three-train scenario is simulated. In this scenario, the load has different types of rapid change from traction consumption to regenerative energy feedback. Only dual-end supply

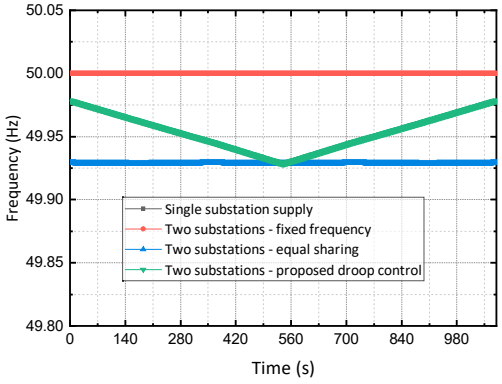

Fig. 8. Comparison of network voltage frequency

schemes are compared because the single end substation cannot support such a heavy load within permissible voltage range.

Fig. 9 shows the total power consumption and the power loss plot of the three dual-end supply approaches. During 0 to 120 s when the load is concentrating at the SS1, the proposed droop control method has the same energy loss as the fixed frequency method. Then during 180 to 240 s when the total traction load exceeds 50 MW, the proposed method has more similar performance with the equal sharing method. And around 300 s the proposed method has medium power loss among the other two. Both fixed frequency method and the proposed one has better efficiency when the load is near to one substation no matter in traction supply or regeneration mode. The difference of these methods become indistinguishable when the equivalent load is in the middle.

The voltage measured at all three trains are plotted in Fig. 10. In the light load condition, all three methods have almost the same voltage drop, but in the heavy load condition, the proposed method and the equal sharing scheme both have greater voltage changes because of evenness of the current from both sides. In the medium load the proposed method has less voltage deviations than the equal sharing. All three schemes can guarantee that train side voltage is above 19 kV which is the lowest permissible voltage.

It can be concluded that the proposed droop control approach is a trade-off between the other two dual-end supply methods. In the lighter condition, the least resistive load character is preserved by the adaptive droop controller based on traction load profiles, timetables or communicated information. When the traction load increases to a certain level (the saturation setpoint), the droop controller gradually relaxes the least power loss objective, and gradually evolves to more evenly load sharing scheme between the two substations.

6. CONCLUSION

With the rapid development of the power converter technology, the AC railway power supply is no longer an isolated system. The system model developed in this paper provides an environment for designing and testing the proposed parallel feeding method. A single track dynamic network simulation platform is built and a special dual-

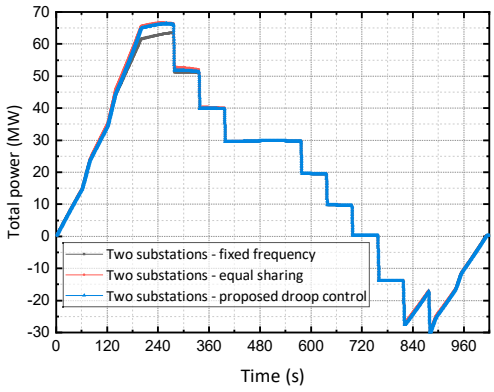

(a) Total power consumption

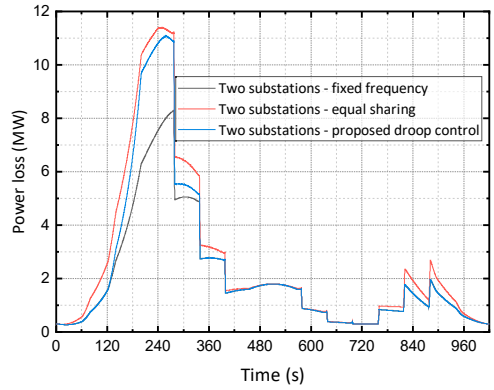

(b) Power loss comparison

Fig. 9. Comparison of active power consumption (three traction load)

end optimal power sharing droop control is proposed. This simulation platform enables a single track AT traction network simulation which supports continuous moving of multiple trains along the track with dynamic load profiles. The voltage measured at the train's pantograph can be tested continuously, and the transient dynamics can be approximately simulated.

The proposed power sharing droop control realises the least power losses supply in the light and medium load conditions. And this approach reduces the rating of each substation for peak load supply. The proposed droop controller is analysed and designed to guarantee the frequency change rate and convergence speed.

A number of simplifications are applied in this preliminary study of the network modelling and power sharing control strategy design. The cross bond impedance is neglected to simplify the modelling procedure when a train continuously move along the line. The saturation effect in each component is not modelled and only linear models are used. The traction load can be improved to incorporate real driving control rather than following the designed power profiles. The model can also incorporate the harmonic issues and the harmonics control research in the parallel SFCs AC supply network. The future work includes the update of the network model to reflect more detailed dynamics. New control strategy might be needed when the number of substations is more than two.

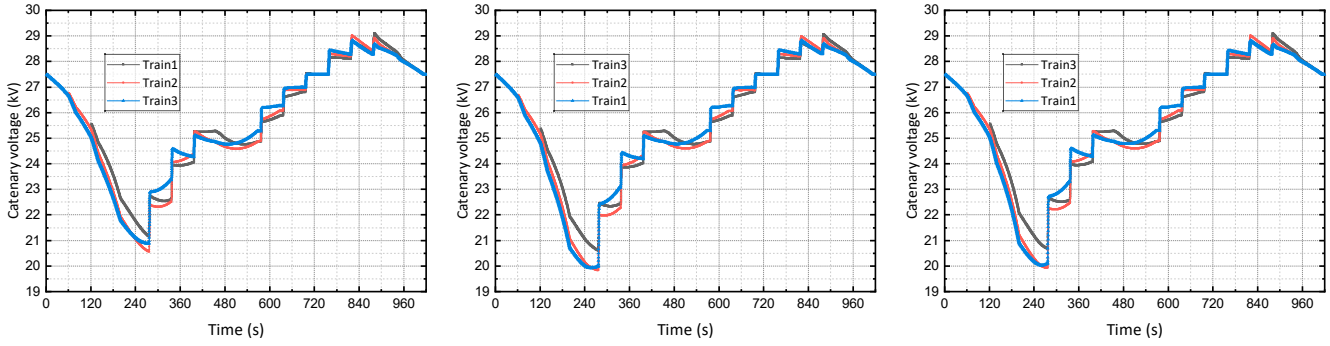

(a) Fixed frequency method (b) Equal sharing method (c) The proposed method

Fig. 10. Train side voltage RMS measurement (three trains)

REFERENCES

Bagnall, T., Siliezar, F., et al. (2014). Power electronics based traction power supply for 50hz railways. *CORE 2014: Rail Transport For A Vital Economy*, 413.

Buttery, A.J., Bagnall, T.M., et al. (2016). Protection and control concepts for sfc fed railways. *CORE 2016: Maintaining the Momentum*, 81.

Chen, J., Wang, L., Diao, L., Du, H., and Liu, Z. (2015). Distributed auxiliary inverter of urban rail train—load sharing control strategy under complicated operation condition. *IEEE Transactions on Power Electronics*, 31(3), 2518–2529.

Gómez-Expósito, A., Mauricio, J.M., and Maza-Ortega, J.M. (2013). Vsc-based mvdc railway electrification system. *IEEE Transactions on power Delivery*, 29(1), 422–431.

Han, P., Wang, Y., Peng, X., He, X., Shu, Z., and Gao, S. (2017). Current-sharing performance of an advanced co-phase traction power substation system based on cascade-parallel converter. In *2017 IEEE 3rd International Future Energy Electronics Conference and ECCE Asia (IFEEC 2017-ECCE Asia)*, 1932–1937. IEEE.

Hao, F., Zhang, G., Chen, J., Liu, Z., Xu, D., and Wang, Y. (2020). Optimal voltage regulation and power sharing in traction power systems with reversible converters. *IEEE Transactions on Power Systems*, 35(4), 2726–2735.

Hu, H., He, Z., Li, X., Wang, K., and Gao, S. (2015). Power-quality impact assessment for high-speed railway associated with high-speed trains using train timetable—part i: Methodology and modeling. *IEEE Transactions on Power Delivery*, 31(2), 693–703.

Junwen, H., Qunzhan, L., Xiaohui, Z., et al. (2010). General mathematical model for simulation of ac traction power supply system and its application. *Power System Technology*, 34(7), 18–23.

Krastev, I., Tricoli, P., Hillmansen, S., and Chen, M. (2016). Future of electric railways: advanced electrification systems with static converters for ac railways. *IEEE Electrification Magazine*, 4(3), 6–14.

Perin, I., Walker, G.R., and Ledwich, G. (2018). Load sharing and wayside battery storage for improving ac railway network performance, with generic model for capacity estimation, part 1. *IEEE Transactions on Industrial Electronics*, 66(3), 1791–1798.

Serrano-Jiménez, D., Abrahamsson, L., Castaño-Solís, S., and Sanz-Feito, J. (2017). Electrical railway power supply systems: Current situation and future trends. *International Journal of Electrical Power & Energy Systems*, 92, 181–192.

Shan, W., Wei, L., and Chen, K. (2017). Longitudinal train dynamics of electric multiple units under rescue. *Journal of modern transportation*, 25, 250–260.

Sharifi, D. (2018). Static frequency converters: the future for railway traction. `https://eress.eu/media/37664/eress-award-dela-sharifi.pdf`.

Sharifi, D., Tricoli, P., and Hillmansen, S. (2016). A new control technique enabling dual-feeding of 50 hz ac railways with static converter feeder stations. In *8th IET International Conference on Power Electronics, Machines and Drives (PEMD 2016)*, 1–7. IET.

Shimizu, T., Kunomura, K., Kai, M., Onishi, M., Masuzawa, H., Miyajima, H., Otsuki, M., and Tsuruma, Y. (2014). The application of electronic frequency converter to the shinkansen railyard power supply. In *2014 International Power Electronics Conference (IPEC-Hiroshima 2014-ECCE ASIA)*, 1054–1061. IEEE.

Steimel, A. (2012). Power-electronic grid supply of ac railway systems. In *2012 13th International Conference on Optimization of Electrical and Electronic Equipment (OPTIM)*, 16–25. IEEE.

Sun, P., Li, K., Li, Y., and Zhang, L. (2020). Dc voltage control for mmc-based railway power supply integrated with renewable generation. *IET Renewable Power Generations*, 14(18), 3679–3689.

Taffese, A.A., Endegnanew, A.G., D'Arco, S., and Tedeschi, E. (2020). Power oscillation damping with virtual capacitance support from modular multilevel converters. *IET Renewable Power Generation*, 14(5), 897–905.